

Observation of azimuth-dependent suppression of hadron pairs in electron scattering off nuclei

S.J. Paul,⁴⁶ S. Morán,⁴⁶ M. Arratia,^{46,42} A. El Alaoui,⁴³ H. Hakobyan,⁴³ W. Brooks,⁴³ M.J. Amarian,³⁴ W.R. Armstrong,¹ H. Atac,⁴¹ L. Baashen,¹³ N.A. Baltzell,⁴² L. Barion,¹⁶ M. Bashkanov,⁴⁸ M. Battaglieri,¹⁸ I. Bedlinskiy,²⁹ B. Benkel,⁴³ F. Benmokhtar,¹⁰ A. Bianconi,^{44,22} L. Biondo,^{18,21,45} A.S. Biselli,^{11,4} M. Bondi,¹⁹ F. Bossù,⁶ S. Boiarinov,⁴² K.-Th. Brinkmann,³⁵ W.J. Briscoe,¹⁵ D. Bulumulla,³⁴ V.D. Burkert,⁴² R. Capobianco,⁸ D.S. Carman,⁴² A. Celentano,¹⁸ V. Chesnokov,³⁹ T. Chetry,¹³ G. Ciullo,^{16,12} P.L. Cole,^{26,5,42} M. Contalbrigo,¹⁶ G. Costantini,^{44,22} A. D'Angelo,^{19,38} N. Dashyan,⁵¹ R. De Vita,¹⁸ M. Defurne,⁶ A. Deur,⁴² S. Diehl,^{35,8} C. Dilks,⁹ C. Djalali,^{33,40} R. Dupre,²³ H. Egiyan,⁴² L. El Fassi,²⁸ P. Eugenio,¹⁴ S. Fegan,⁴⁸ A. Filippi,²⁰ G. Gavalian,^{42,30} Y. Ghandilyan,⁵¹ G.P. Gilfoyle,³⁷ A.A. Golubenkov,³⁹ G. Gosta,⁴⁴ R.W. Gothe,⁴⁰ K.A. Griffioen,⁵⁰ M. Guidal,²³ M. Hattawy,³⁴ T.B. Hayward,⁸ D. Heddle,^{7,42} A. Hobart,²³ M. Holtrop,³⁰ Y. Ilieva,^{40,15} D.G. Ireland,⁴⁷ E.L. Isupov,³⁹ H.S. Jo,²⁵ R. Johnston,²⁷ K. Joo,⁸ S. Joosten,¹ D. Keller,⁴⁹ A. Khanal,¹³ M. Khandaker,^{32,*} W. Kim,²⁵ A. Kripko,³⁵ V. Kubarovsky,⁴² V. Lagerquist,³⁴ L. Lanza,¹⁹ M. Leali,^{44,22} S. Lee,²⁷ P. Lenisa,^{16,12} X. Li,²⁷ K. Livingston,⁴⁷ I.J.D. MacGregor,⁴⁷ D. Marchand,²³ V. Mascagna,^{44,22} B. McKinnon,⁴⁷ Z.E. Meziani,¹ S. Migliorati,^{44,22} R.G. Milner,²⁷ T. Mineeva,⁴³ M. Mirazita,¹⁷ V.I. Mokeev,⁴² P. Moran,²⁷ C. Munoz Camacho,²³ K. Neupane,⁴⁰ D. Nguyen,⁴² S. Niccolai,²³ G. Niclescu,²⁴ M. Osipenko,¹⁸ A.I. Ostrovidov,¹⁴ P. Pandey,³⁴ M. Paolone,³¹ L.L. Pappalardo,^{16,12} R. Paremuzyan,^{42,30} E. Pasyuk,⁴² W. Phelps,⁷ N. Pilleux,²³ D. Pocanic,⁴⁹ O. Pogorelko,²⁹ M. Pokhrel,³⁴ J. Poudel,³⁴ J.W. Price,² Y. Prok,^{34,49} B.A. Raue,¹³ T. Reed,¹³ M. Ripani,¹⁸ G. Rosner,⁴⁷ F. Sabatié,⁶ C. Salgado,³² A. Schmidt,¹⁵ R.A. Schumacher,⁴ Y.G. Sharabian,⁴² E.V. Shirokov,³⁹ U. Shrestha,⁸ P. Simmerling,⁸ D. Sokhan,^{6,47} N. Sparveris,⁴¹ S. Stepanyan,⁴² I.I. Strakovsky,¹⁵ S. Strauch,^{40,15} J.A. Tan,²⁵ R. Tyson,⁴⁷ M. Ungaro,^{42,36} S. Vallarino,¹⁶ L. Venturelli,^{44,22} H. Voskanyan,⁵¹ E. Voutier,²³ X. Wei,⁴² R. Wishart,⁴⁷ M.H. Wood,^{3,40} N. Zachariou,⁴⁸ Z.W. Zhao,⁹ V. Ziegler,⁴² and M. Zurek¹

(The CLAS Collaboration)

¹Argonne National Laboratory, Argonne, Illinois 60439

²California State University, Dominguez Hills, Carson, CA 90747

³Canisius College, Buffalo, NY

⁴Carnegie Mellon University, Pittsburgh, Pennsylvania 15213

⁵Catholic University of America, Washington, D.C. 20064

⁶IRFU, CEA, Université Paris-Saclay, F-91191 Gif-sur-Yvette, France

⁷Christopher Newport University, Newport News, Virginia 23606

⁸University of Connecticut, Storrs, Connecticut 06269

⁹Duke University, Durham, North Carolina 27708-0305

¹⁰Duquesne University, 600 Forbes Avenue, Pittsburgh, PA 15282

¹¹Fairfield University, Fairfield CT 06824

¹²Università di Ferrara, 44121 Ferrara, Italy

¹³Florida International University, Miami, Florida 33199

¹⁴Florida State University, Tallahassee, Florida 32306

¹⁵The George Washington University, Washington, DC 20052

¹⁶INFN, Sezione di Ferrara, 44100 Ferrara, Italy

¹⁷INFN, Laboratori Nazionali di Frascati, 00044 Frascati, Italy

¹⁸INFN, Sezione di Genova, 16146 Genova, Italy

¹⁹INFN, Sezione di Roma Tor Vergata, 00133 Rome, Italy

²⁰INFN, Sezione di Torino, 10125 Torino, Italy

²¹INFN, Sezione di Catania, 95123 Catania, Italy

²²INFN, Sezione di Pavia, 27100 Pavia, Italy

²³Université Paris-Saclay, CNRS/IN2P3, IJCLab, 91405 Orsay, France

²⁴James Madison University, Harrisonburg, Virginia 22807

²⁵Kyungpook National University, Daegu 41566, Republic of Korea

²⁶Lamar University, 4400 MLK Blvd, PO Box 10046, Beaumont, Texas 77710

²⁷Massachusetts Institute of Technology, Cambridge, Massachusetts 02139-4307

²⁸Mississippi State University, Mississippi State, MS 39762-5167

²⁹National Research Centre Kurchatov Institute - ITEP, Moscow, 117259, Russia

³⁰University of New Hampshire, Durham, New Hampshire 03824-3568

- ³¹*New Mexico State University, PO Box 30001, Las Cruces, NM 88003, USA*
³²*Norfolk State University, Norfolk, Virginia 23504*
³³*Ohio University, Athens, Ohio 45701*
³⁴*Old Dominion University, Norfolk, Virginia 23529*
³⁵*II Physikalisches Institut der Universitaet Giessen, 35392 Giessen, Germany*
³⁶*Rensselaer Polytechnic Institute, Troy, New York 12180-3590*
³⁷*University of Richmond, Richmond, Virginia 23173*
³⁸*Università di Roma Tor Vergata, 00133 Rome Italy*
³⁹*Skobeltsyn Institute of Nuclear Physics, Lomonosov Moscow State University, 119234 Moscow, Russia*
⁴⁰*University of South Carolina, Columbia, South Carolina 29208*
⁴¹*Temple University, Philadelphia, PA 19122*
⁴²*Thomas Jefferson National Accelerator Facility, Newport News, Virginia 23606*
⁴³*Universidad Técnica Federico Santa María, Casilla 110-V Valparaíso, Chile*
⁴⁴*Università degli Studi di Brescia, 25123 Brescia, Italy*
⁴⁵*Università degli Studi di Messina, 98166 Messina, Italy*
⁴⁶*University of California Riverside, 900 University Avenue, Riverside, CA 92521, USA*
⁴⁷*University of Glasgow, Glasgow G12 8QQ, United Kingdom*
⁴⁸*University of York, York YO10 5DD, United Kingdom*
⁴⁹*University of Virginia, Charlottesville, Virginia 22901*
⁵⁰*College of William and Mary, Williamsburg, Virginia 23187-8795*
⁵¹*Yerevan Physics Institute, 375036 Yerevan, Armenia*

We present the first measurement of di-hadron angular correlations in electron-nucleus scattering. The data were taken with the CLAS detector and a 5.0 GeV electron beam incident on deuterium, carbon, iron, and lead targets. Relative to deuterium, the nuclear yields of charged-pion pairs show a strong suppression for azimuthally opposite pairs, no suppression for azimuthally nearby pairs, and an enhancement of pairs with large invariant mass. These effects grow with increased nuclear size. The data are qualitatively described by the GiBUU model, which suggests that hadrons form near the nuclear surface and undergo multiple-scattering in nuclei. These results show that angular correlation studies can open a new way to elucidate how hadrons form and interact inside nuclei.

Introduction. The quark-to-hadron transition, called hadronization, remains poorly understood in part due to the great challenge it poses to first-principle calculations in quantum chromodynamics. Studying how hadronization occurs inside large nuclei provides a way to perturb the process to potentially reveal its mechanisms and timescales [1–4]. It also represents a way to probe the transport properties of nuclei [5–12], and tune models needed to interpret neutrino experiments [13, 14].

Scattering experiments with electron beams can help elucidate hadron production by providing control over the energy, ν , and momentum, \vec{q} , transferred in the reaction, which is determined from the scattered electron. Previous studies by HERMES [15–19] and CLAS [20, 21] experiments revealed that the production of hadrons is strongly suppressed in nuclei, with a complex dependence on the hadron’s energy, transverse momentum, and type. These data agree with various models that include either gluon bremsstrahlung, hadron re-scattering and absorption, or a mixture of these [1].

Di-hadron measurements can complement single-hadron studies by providing more kinematic variables and higher sensitivity to nuclear effects such as multiple scattering [22–28]. Such variables include angular correlations, which were measured in hadron-collider and

fixed-target experiments to probe cold and hot nuclear matter (see Refs. [1, 29] for reviews). No analogous study has been done with electron beams.

Given the strong absorption of hadrons in nuclei [15–21], it is expected that most observed hadrons correspond to those that were created near the nuclear surface [30] and have their momentum directed away from the center of the nucleus. Detailed modelling of such geometrical effects remains a challenge [7]. Di-hadron azimuthal correlations offer a way to test this hypothesis. When hadron pairs are produced near the surface and off-axis from the nuclear center, the shortest path lengths through the nucleus are obtained when both hadrons’ transverse momenta are directed away from the center of the nucleus relative to their production positions. When averaging over possible initial-production positions in the nucleus, this favors events in which the azimuthal separation between the hadrons is small, while suppressing those with large azimuthal separation (see Fig. 1). Such a “surface bias” has been observed in hadron collisions and has been exploited as a tool to study cold and hot nuclear matter [29].

The di-hadron measurements at HERMES [31] revealed hints of nuclear suppression, although with limited precision; moreover, those studies did not explore angular dependence nor did they include hadron iden-

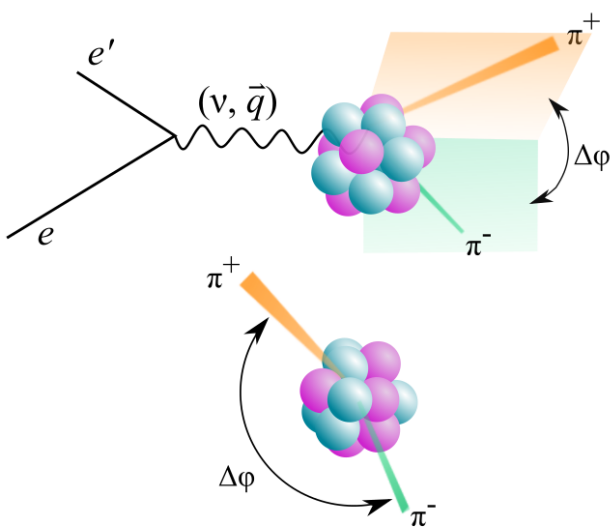


Figure 1. Diagram illustrating di-pion production in a nucleus. Top: side-view, illustrating that the momentum-transfer axis is used to define the azimuthal separation, $\Delta\phi$. Bottom: same reaction, as viewed from the direction of the momentum transfer.

tification, which was crucial to elucidate single-hadron studies [16, 17, 19]. Di-hadron measurements were also performed in the SKAT experiment [32], which used a neutrino beam incident on heavy nuclei.

We build upon the HERMES results by studying di-hadron production with a much higher precision and with identified hadrons; in addition, we measure for the first time the di-hadron suppression as a function of the azimuthal separation and the invariant mass. In particular, we study the reaction

$$eA \rightarrow e'\pi^+\pi^-X, \quad (1)$$

where X represents other particles in the event.

Experimental setup. The data presented here were collected at the Continuous Electron Beam Accelerator Facility (CEBAF) Large Acceptance Spectrometer (CLAS) with a 5.0 GeV electron beam incident on a dual-target system [33] consisting of a liquid ^2H target cell and a C, Fe, or Pb foil target.

The CLAS [34] detector was based on a six-fold symmetric toroidal magnet, which defined six sectors instrumented with drift chambers (DC), time-of-flight scintillation counters (TOF), Cherenkov counters (CC), and an electromagnetic calorimeter (EC). Following Refs. [21, 35], electrons were identified by matching negatively charged tracks measured in the DC with hits in the TOF and EC. Background from π^- was suppressed to the $< 1\%$ level using the CC and the EC. Charged-pions were identified with TOF hits consistent with charged pions with momentum determined in

the DCs. The selection for π^+ with momentum above 2.7 GeV was further refined with the CC to suppress proton background. Fiducial cuts on momentum and angles were used in order to avoid regions with steeply varying acceptance or low resolution.

Event selection and observables. The data were selected with a trigger that required at least one electron candidate with momentum $p > 500$ MeV. Similar to Ref. [21], we selected events with $Q^2 > 1 \text{ GeV}^2$, $W > 2 \text{ GeV}$ and $2.2 < \nu < 4.2 \text{ GeV}$. Here, Q^2 is the square of the four-momentum transfer, $W = \sqrt{2m_p\nu + m_p^2 - Q^2}$ where m_p is the mass of a proton, $\nu = E - E'$ is the energy transfer, and E and E' are the beam- and scattered-electron energies.

Following Ref. [31], we selected events with a “leading” pion, defined as having fractional energy $z_1 = E_h/\nu > 0.5$, where E_h is the energy of the pion; we then measured all the other (“secondary”) pions in the event with charge opposite that of the leading pion in the fractional-energy range $0.05 < z_2 < 0.45$. In addition, we removed kinematically forbidden events by requiring $|p_1| + |p_2| < \nu$, where p_1 and p_2 are the momenta of the pion candidates, in order to suppress proton background. The selection included both resonant and non-resonant di-pion production, including exclusive processes, as well as secondary hadrons arising from hadron re-scattering and other nuclear interactions.

We selected particles arising from scattering from either the deuterium or nuclear targets by using the longitudinal vertex position defined by intersecting their trajectories with the beamline. The resulting vertex resolution ensured negligible ambiguity in the target tagging [21].

We used the electron, the leading pion, and the sub-leading pion variables to measure the conditional modification factor, R_{2h} , defined [31] as:

$$R_{2h}(z_2) = \frac{(dN_{2h}^A(z_2)/dz_2)/N_h^A}{(dN_{2h}^D(z_2)/dz_2)/N_h^D}. \quad (2)$$

Here, $(dN_{2h}(z_2)/dz_2)/N_h$ is the ratio of the differential number of selected events with a secondary hadron with energy fraction z_2 , a leading pion, and an electron, to the total number of selected events with an electron and a leading pion. In other words, R_{2h} is the nuclear-to-deuterium ratio of the average number of secondary pions per leading pion. The superscript indicates that the term is calculated for a nuclear (A) or deuterium (D) target. Likewise, we also measured R_{2h} in this work as a function of the azimuthal separation between the pions, $|\Delta\phi|$, and the di-pion invariant mass, $m_{\pi\pi}$.

Uncertainties. By construction, R_{2h} is a double ratio that benefits from the cancellation of various corrections for detector effects and thus minimizes the associ-

ated systematic uncertainties. Moreover, we exploited the dual-target system [36], which by design minimizes systematic uncertainties related to variations in detector response over time by exposing the deuterium and heavier nuclear targets at the same time. This feature of the dual target has been exploited in various studies [20, 21, 35, 37–44] which used the same data set as this work.

We performed studies on various possible sources of systematic uncertainties using data and simulation studies. For the simulation studies we used the PYTHIA 6.319 event generator and the GSIM package [45], which is based on GEANT3 [46], to simulate the response of the CLAS detector and dual-target setup [33]. The simulation was tuned to provide a reasonable description of the data. The possible sources of systematic uncertainties studied include acceptance effects, event selection, particle mis-identification, and radiative effects. Other sources of systematic uncertainty, such as cross contamination between bins, beam luminosity, trigger efficiency, Coulomb effects, and time-dependent effects, were found to be negligible.

The systematic uncertainties from different sources were added in quadrature, and totaled to 2.5–3.0% for most bins. However, for some bins, in particular at high $m_{\pi\pi}$, they reached 8.6%. In this region, the large systematic uncertainty is largely due to momentum-dependent variations in the efficiency of the CC, which we used to distinguish between high-momentum π^+ and protons. For most bins, the systematic uncertainty dominated over the statistical uncertainty, which ranged from 1.1–12%, with a median value of 2.6%.

Results and discussion. Figure 2(a) shows results for R_{2h} as a function of the fractional energy of the sub-leading pion of the pair, z_2 . The CLAS data show a suppression for almost all of the bins, with stronger suppression for heavier nuclei. R_{2h} depends weakly on z_2 except at the first and last bins. The values of R_{2h} for Fe and Pb appear close; however, a χ^2 test reveals that their differences are significant at the 99% CL¹. In the $0.1 < z_2 < 0.4$ range, the average values of R_{2h} are $0.836 \pm 0.007 \pm 0.024$, $0.738 \pm 0.005 \pm 0.021$, and $0.698 \pm 0.008 \pm 0.020$ for C, Fe, and Pb, respectively (where the first uncertainty is statistical and the second is systematic).

Our data in Fig 2(a) are compared with existing eA and νA data from the HERMES [31] and SKAT [32] experiments, respectively. The average kinematics for

our results are $\langle\nu\rangle = 3.3$ GeV and $\langle Q^2\rangle = 1.6$ GeV², whereas the HERMES results were at $\langle\nu\rangle = 17.7$ GeV and $\langle Q^2\rangle = 2.4$ GeV² [31]. The SKAT data were taken at $\langle\nu\rangle = 5.8$ GeV and $\langle Q^2\rangle = 2.7$ GeV² [32]. The significant differences observed suggest that the change of kinematics has a strong impact on the nuclear effects. Unlike HERMES, our results show significant evidence for a dependence on the nuclear mass.

Furthermore, the differences between the HERMES and CLAS results may be explained by the smaller energy transfer in the latter, causing the hadron-formation length to be shorter. This increases the distance that the hadrons have to travel to escape, increasing the probability of their absorption. In the HERMES case, there is an increased probability of pions forming outside of the nucleus, due to longer hadron-formation lengths compared to the CLAS case.

We compare our data with the GIBUU Monte-Carlo event generator [48] (using the 2019 default parameters), which incorporates treatment of final-state interactions, absorption, and production mechanisms with elastic and inelastic channels. The GIBUU model described reasonably well the single-hadron data from CLAS [21] and HERMES [16, 17, 19]. While the GIBUU calculations reproduce some of the qualitative features of the data in this work, there are significant differences, for instance it predicts an uptick only at low z_2 , while the data have an uptick at both the lowest and the highest z_2 bins. The low- z_2 uptick was also observed in the HERMES and SKAT data, which were at very different kinematics, suggesting that this effect does not depend strongly on Q^2 or ν . In the GIBUU model, the uptick in R_{2h} at low z_2 is produced as a consequence of the interaction between hadrons produced in the primary electron-nucleon interaction with other hadrons as they propagate through nuclei. The uptick at high z_2 is consistent with unity and also exists in the HERMES results. This high- z_2 uptick, which is not reproduced by the GIBUU model, may be due to coherent production in the $z_1 + z_2 \rightarrow 1$ limit; coherent production in general is not included in the GIBUU model [48].

Figure 2(b) shows R_{2h} as a function of the azimuthal separation, $\Delta\phi$, between the two pions, as measured around the direction of the momentum transfer (see Fig. 1). The data show significant dependence on $\Delta\phi$ for all nuclei. For all three nuclei, the deviation of R_{2h} from unity is smallest when $\Delta\phi$ is near 0 and drops off with increasing $|\Delta\phi|$, with a steeper slope for heavier nuclei. For azimuthally opposite pairs ($|\Delta\phi|$ near π), R_{2h} is $0.789 \pm 0.013 \pm 0.024$, $0.671 \pm 0.010 \pm 0.020$, and $0.620 \pm 0.015 \pm 0.026$ for C, Fe, and Pb, respectively. This is qualitatively described by the GIBUU model;

¹ For this test, only the statistical uncertainties were considered, since the systematic uncertainties were assumed to be fully correlated between the different nuclei for any given bin.

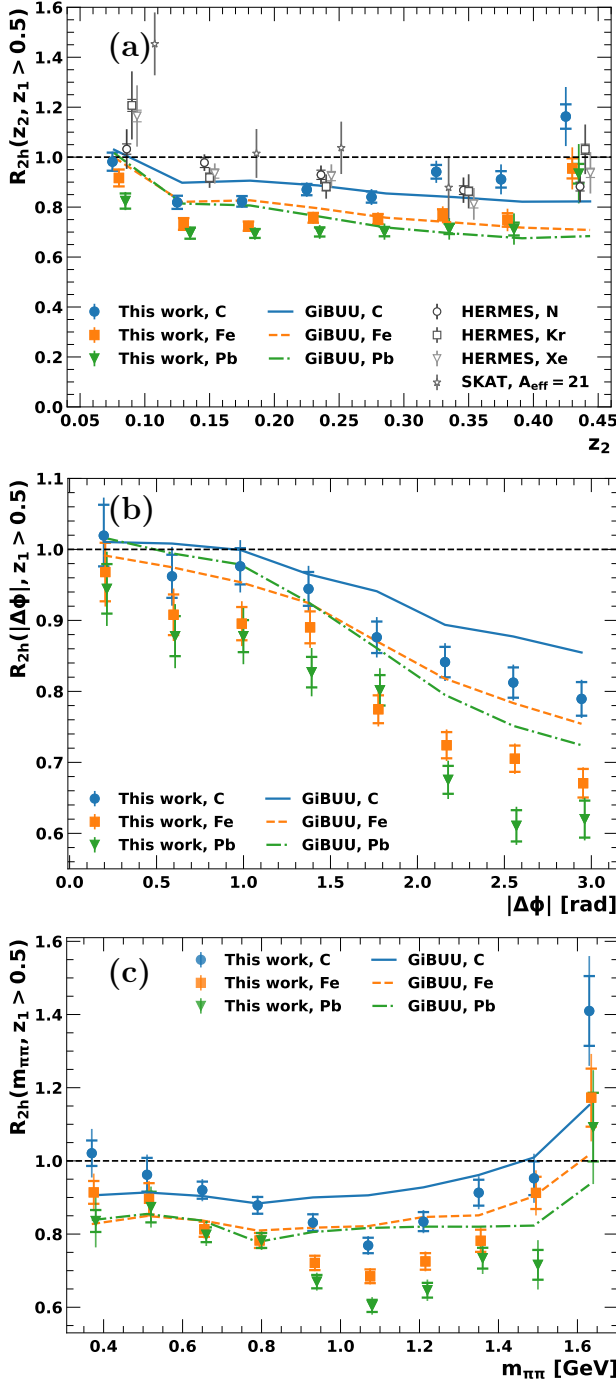


Figure 2. Conditional suppression factor, R_{2h} , as a function of (a) sub-leading hadron z , (b) the azimuthal separation $|\Delta\phi|$, and (c) the invariant mass of the pion pair. Points are slightly shifted horizontally for visibility. The gray open symbols in (a) represent results by the HERMES [31] and SKAT [32] experiments. Horizontal bars represent the systematic uncertainties, while the vertical bars represent the total systematic and statistical uncertainty (added in quadrature). The values of R_{2h} , statistical and systematic uncertainties, and bin edges are tabulated in the Supplementary Material [47]. Curves represent the calculations from the GiBUU model [48].

however, the data show a more pronounced $\Delta\phi$ dependence.

We also present R_{2h} as a function of the di-pion invariant mass, $m_{\pi\pi}$, in Fig. 2(c). The data show a negative slope in the $0.4 < m_{\pi\pi} < 1.1$ GeV region, and an enhancement at higher $m_{\pi\pi}$. We also observe that within the region of negative slope, the dependence appears to be smooth and no abrupt behavior is observed in R_{2h} near the $\rho^0(770)$ mass. The data are qualitatively described by GiBUU, including the uptick at high mass. In the GiBUU model, this is a product of the re-scattering of hadrons, which leads to larger transverse momentum of hadrons and higher pair invariant mass. The qualitative behavior of the data is reminiscent of the enhancement of hadrons with high-transverse momentum reported in Refs. [15–19, 21, 49].

Hadron-absorption effects in the GiBUU model can be investigated through looking at the distribution of the hadron-production points of the final-state pions. We observe that in the GiBUU simulations, a larger fraction of the total final-state pions are formed near the surface of the nucleus than would be expected if their production points were distributed uniformly. Further, we observe that this effect is stronger for larger nuclei than for smaller ones. The effect is also stronger in the di-pion case than for the single-pion case. The latter effect can be explained by the fact that we require the survival of not only the secondary pion but also the leading one as well, biasing the sample further towards the surface. Such an interpretation is consistent with Ref. [30], which argued that an absorption model coupled with geometrical biases caused by survivor selection could explain both the single and double-hadron data from HERMES without resorting to other effects such as gluon bremsstrahlung [50, 51].

Summary and conclusions. In summary, we have presented a measurement of di-pion production in electron scattering off nuclei using the CLAS detector, which includes the first study on the azimuthal separation and invariant mass. The data show a strong suppression for azimuthally opposite pairs, no suppression for pairs that are close in azimuthal angle, and an enhancement of pairs with large invariant mass. This is qualitatively consistent with the predictions from the GiBUU model, wherein it can be attributed to an increased probability of absorption of hadrons in azimuthally opposite pairs due to the increased path length compared to azimuthally nearby pairs; however, the measured suppression is stronger than in the predictions.

We also measured the dependence of the nuclear-to-deuterium ratio on the secondary pion’s fractional energy, and on the di-pion invariant mass. We compared

our measurement of the dependence on the former with results from HERMES and found both to be qualitatively comparable; however, our measurement shows a stronger nuclear dependence than the HERMES results, which suggests a strong kinematic dependence of the observed effects. Further, we note that the di-hadron suppression is stronger in heavier nuclei, although the effect appears to saturate for higher nuclear masses.

Overall, the data show evidence that nuclear effects not only modify the hadron distributions, but also modify the correlations between multiple hadrons in the event, relative to the correlations that exist in the deuteron case due to momentum conservation and limited phase space.

Our studies show how kinematic variables that depend on both hadrons, such as azimuthal separation and pair mass, can be used as a powerful tool for studying hadron production in electron scattering off nuclei. Given that these data cover a poorly explored kinematic domain where the hadron-formation length is expected to be similar to the nuclear size, future comparisons to models (similar to those of Refs. [52, 53]) might shed light on hadronization timescales and mechanisms.

These results provide a reference for planned di-hadron measurements in future experiments with higher beam energies at the Jefferson Laboratory [54–56], and future electron-ion colliders in the USA [2, 57] and China [58].

Acknowledgements. The authors acknowledge the staff of the Accelerator and Physics Divisions at the Thomas Jefferson National Accelerator Facility who made this experiment possible. We thank Kai Gallmeister for help in setting up the GiBUU event generator. This work was supported in part by the Chilean Agencia Nacional de Investigacion y Desarrollo (ANID), by ANID PIA grant ACT1413, by ANID PIA/APOYO AFB180002, by ANID FONDECYT No. 1161642 and No. 1201964 and No. 11181215 and No. 1151248, by the ANID-Millennium Science Initiative Program - ICN2019_044, by the U.S. Department of Energy, the Italian Istituto Nazionale di Fisica Nucleare, the French Centre National de la Recherche Scientifique, the French Commissariat à l’Energie Atomique, the United Kingdom Science and Technology Facilities Council (STFC), the Scottish Universities Physics Alliance (SUPA), the National Research Foundation of Korea, the National Science Foundation (NSF), the HelmholtzForschungsakademie Hessen für FAIR (HFHF), the Ministry of Science and Higher Education of the Russian Federation, and the Office of Research and Economic Development at Mississippi State University. This work has received funding from the European Research Council (ERC) under

the European Union’s Horizon 2020 research and innovation programme (Grant agreement No. 804480). The Southeastern Universities Research Association operates the Thomas Jefferson National Accelerator Facility for the United States Department of Energy under Contract No. DE-AC05-06OR23177.

-
- * Current address: Idaho State University, Pocatello, Idaho 83209
- [1] A. Accardi, F. Arleo, W. K. Brooks, D. D’Enterria, and V. Muccifora, *Riv. Nuovo Cim.* **32**, 439 (2009).
 - [2] A. Accardi *et al.*, *Eur. Phys. J.* **A52**, 268 (2016).
 - [3] M. Y. Barabanov *et al.*, *Prog. Part. Nucl. Phys.* **116**, 103835 (2021).
 - [4] W. K. Brooks and J. A. López, *Phys. Lett. B* **816**, 136171 (2021).
 - [5] R. Baier, Y. L. Dokshitzer, A. H. Mueller, S. Peigné, and D. Schiff, *Nucl. Phys. B* **484**, 265 (1997).
 - [6] X. Guo and X.-N. Wang, *Phys. Rev. Lett.* **85**, 3591 (2000).
 - [7] N. Liu, W.-D. Miao, L.-H. Song, and C.-G. Duan, *Phys. Lett. B* **749**, 88 (2015).
 - [8] R. Dupré and S. Scopetta, *Eur. Phys. J. A* **52**, 159 (2016), [arXiv:1510.00794 \[nucl-ex\]](#).
 - [9] L.-H. Song, S.-F. Xin, and N. Liu, *J. Phys.* **G45**, 025005 (2018).
 - [10] P. Ru, Z.-B. Kang, E. Wang, H. Xing, and B.-W. Zhang, *Phys. Rev. D* **103**, L031901 (2021).
 - [11] T.-X. Bai and C.-G. Duan, *Eur. Phys. J. Plus* **136**, 1181 (2021).
 - [12] B. Guiot and B. Z. Kopeliovich, *Phys. Rev. C* **102**, 045201 (2020).
 - [13] L. Alvarez-Ruso *et al.*, *Prog. Part. Nucl. Phys.* **100**, 1 (2018).
 - [14] U. Mosel, *J. Phys.* **G46**, 113001 (2019).
 - [15] A. Airapetian *et al.* (HERMES Collaboration), *Eur. Phys. J.* **C20**, 479 (2001).
 - [16] A. Airapetian *et al.* (HERMES Collaboration), *Phys. Lett.* **B577**, 37 (2003).
 - [17] A. Airapetian *et al.* (HERMES Collaboration), *Nucl. Phys.* **B780**, 1 (2007).
 - [18] A. Airapetian *et al.* (HERMES Collaboration), *Phys. Lett.* **B684**, 114 (2010).
 - [19] A. Airapetian *et al.* (HERMES Collaboration), *Eur. Phys. J.* **A47**, 113 (2011).
 - [20] A. Daniel *et al.* (CLAS Collaboration), *Phys. Lett.* **B706**, 26 (2011).
 - [21] S. Morán *et al.* (CLAS Collaboration), *Phys. Rev. C* **105**, 015201 (2022).
 - [22] H. Xing, Z.-B. Kang, I. Vitev, and E. Wang, *Phys. Rev. D* **86**, 094010 (2012).
 - [23] F. Cougoulic and S. Peigné, *JHEP* **05**, 203 (2018).
 - [24] Z.-t. Liang, X.-N. Wang, and J. Zhou, *Phys. Rev. D* **77**, 125010 (2008).
 - [25] A. Schäfer and J. Zhou, *Phys. Rev. D* **88**, 074012 (2013).
 - [26] D. Boer, M. Buffing, and P. Mulders, *JHEP* **08**, 053 (2015).

- [27] Y.-Y. Zhang, G.-Y. Qin, and X.-N. Wang, *Phys. Rev. D* **100**, 074031 (2019).
- [28] M. Alrashed, D. Anderle, Z.-B. Kang, J. Terry, and H. Xing, (2021), [arXiv:2107.12401 \[hep-ph\]](#).
- [29] M. Connors, C. Nattrass, R. Reed, and S. Salur, *Rev. Mod. Phys.* **90**, 025005 (2018).
- [30] K. Fialkowski and R. Wit, *Eur. Phys. J. A* **32**, 213 (2007).
- [31] A. Airapetian *et al.* (*HERMES Collaboration*), *Phys. Rev. Lett.* **96**, 162301 (2006).
- [32] N. Agababyan, V. Ammosov, M. Atayan, L. Grigoryan, N. Grigoryan, H. Gulkanyan, A. Ivanilov, Z. Karamyan, and V. Korotkov, *Phys. Atom. Nucl.* **74**, 246 (2011).
- [33] H. Hakobyan, *Observation of Quark Propagation Pattern in Nuclear Medium*, *Ph.D. thesis*, Yerevan State U. (2008).
- [34] B. A. Mecking *et al.* (*CLAS Collaboration*), *Nucl. Instrum. Meth. A* **503**, 513 (2003).
- [35] L. El Fassi *et al.* (*CLAS Collaboration*), *Phys. Lett. B* **712**, 326 (2012).
- [36] H. Hakobyan *et al.*, *Nucl. Instrum. Meth. A* **592**, 218 (2008).
- [37] O. Hen *et al.* (*CLAS Collaboration*), *Phys. Lett. B* **722**, 63 (2013).
- [38] O. Hen *et al.* (*CLAS Collaboration*), *Science* **346**, 614 (2014).
- [39] M. Duer *et al.* (*CLAS Collaboration*), *Phys. Rev. Lett.* **122**, 172502 (2019).
- [40] E. Cohen *et al.* (*CLAS Collaboration*), *Phys. Rev. Lett.* **121**, 092501 (2018).
- [41] M. Duer *et al.* (*CLAS Collaboration*), *Phys. Lett. B* **797**, 134792 (2019).
- [42] B. Schmookler *et al.* (*CLAS Collaboration*), *Nature* **566**, 354 (2019).
- [43] I. Korover *et al.* (*CLAS Collaboration*), (2020), [arXiv:2004.07304 \[nucl-ex\]](#).
- [44] A. Schmidt *et al.* (*CLAS Collaboration*), *Nature* **578**, 540 (2020).
- [45] E. Wolin, “GSIM User’s Guide Version CERN 1.0,” (1995).
- [46] R. Brun, F. Bruyant, F. Carminati, S. Giani, M. Maire, A. McPherson, G. Patrick, and L. Urban, (1994), [10.17181/CERN.MUHF.DMJ1](#).
- [47] See Supplemental Material at [insert URL here] for tables of the conditional modification factor, statistical and systematic uncertainties, and the bin edges.
- [48] O. Buss, T. Gaitanos, K. Gallmeister, H. van Hees, M. Kaskulov, O. Lalakulich, A. B. Larionov, T. Leitner, J. Weil, and U. Mosel, *Phys. Rept.* **512**, 1 (2012).
- [49] A. Airapetian *et al.* (*HERMES Collaboration*), *Phys. Lett. B* **684**, 114 (2010), [arXiv:0906.2478 \[hep-ex\]](#).
- [50] A. Majumder and X.-N. Wang, (2008), [arXiv:0806.2653 \[nucl-th\]](#).
- [51] A. Majumder, *Phys. Rev. D* **85**, 014023 (2012), [arXiv:0912.2987 \[nucl-th\]](#).
- [52] K. Gallmeister and U. Mosel, *Nuclear Physics A* **801**, 68 (2008).
- [53] A. B. Larionov and M. Strikman, *Phys. Rev. C* **101**, 014617 (2020).
- [54] V. D. Burkert, *Ann. Rev. Nucl. Part. Sci.* **68**, 405 (2018).
- [55] V. D. Burkert *et al.*, *Nucl. Instrum. Meth. A* **959**, 163419 (2020).
- [56] J. Arrington *et al.*, (2021), [arXiv:2112.00060 \[nucl-ex\]](#).
- [57] R. Abdul Khalek *et al.*, (2021), [arXiv:2103.05419 \[physics.ins-det\]](#).
- [58] D. P. Anderle *et al.*, *Front. Phys. (Beijing)* **16**, 64701 (2021).

SUPPLEMENTAL MATERIAL

The values of R_{2h} , shown in Fig. 2, are listed in Tables I, II, and III, along with the edges of the bins, and the statistical and systematic uncertainties.

Table I. Values of R_{2h} obtained for each target and each z_2 bin \pm the statistical uncertainty for each data point \pm the systematic uncertainty for each data point. These data correspond to those shown in Fig. 2(a)

z_2	$R_{2h}(\text{C}, z_2)$	$R_{2h}(\text{Fe}, z_2)$	$R_{2h}(\text{Pb}, z_2)$
0.05–0.10	$0.982 \pm 0.017 \pm 0.036$	$0.917 \pm 0.015 \pm 0.034$	$0.824 \pm 0.020 \pm 0.030$
0.10–0.15	$0.819 \pm 0.010 \pm 0.026$	$0.732 \pm 0.008 \pm 0.024$	$0.696 \pm 0.013 \pm 0.022$
0.15–0.20	$0.823 \pm 0.014 \pm 0.021$	$0.724 \pm 0.011 \pm 0.019$	$0.694 \pm 0.017 \pm 0.018$
0.20–0.25	$0.870 \pm 0.018 \pm 0.023$	$0.757 \pm 0.014 \pm 0.020$	$0.700 \pm 0.021 \pm 0.018$
0.25–0.30	$0.840 \pm 0.022 \pm 0.022$	$0.752 \pm 0.018 \pm 0.020$	$0.702 \pm 0.026 \pm 0.019$
0.30–0.35	$0.941 \pm 0.035 \pm 0.027$	$0.769 \pm 0.026 \pm 0.022$	$0.713 \pm 0.038 \pm 0.021$
0.35–0.40	$0.911 \pm 0.050 \pm 0.033$	$0.749 \pm 0.036 \pm 0.027$	$0.712 \pm 0.057 \pm 0.026$
0.40–0.45	$1.163 \pm 0.108 \pm 0.049$	$0.955 \pm 0.074 \pm 0.040$	$0.934 \pm 0.112 \pm 0.039$

Table II. Values of R_{2h} obtained for each target and each $|\Delta\phi|$ bin \pm the statistical uncertainty for each data point \pm the systematic uncertainty for each data point. These data correspond to those shown in Fig. 2(b)

$ \Delta\phi $ [rad]	$R_{2h}(\text{C}, \Delta\phi)$	$R_{2h}(\text{Fe}, \Delta\phi)$	$R_{2h}(\text{Pb}, \Delta\phi)$
0.00–0.39	$1.019 \pm 0.031 \pm 0.043$	$0.968 \pm 0.026 \pm 0.041$	$0.944 \pm 0.039 \pm 0.035$
0.39–0.79	$0.962 \pm 0.028 \pm 0.030$	$0.908 \pm 0.023 \pm 0.029$	$0.878 \pm 0.035 \pm 0.028$
0.79–1.18	$0.976 \pm 0.027 \pm 0.026$	$0.895 \pm 0.021 \pm 0.023$	$0.878 \pm 0.033 \pm 0.023$
1.18–1.57	$0.944 \pm 0.022 \pm 0.024$	$0.890 \pm 0.018 \pm 0.022$	$0.827 \pm 0.026 \pm 0.021$
1.57–1.96	$0.876 \pm 0.018 \pm 0.022$	$0.775 \pm 0.014 \pm 0.020$	$0.802 \pm 0.023 \pm 0.021$
1.96–2.35	$0.841 \pm 0.016 \pm 0.021$	$0.724 \pm 0.012 \pm 0.018$	$0.675 \pm 0.018 \pm 0.020$
2.35–2.75	$0.812 \pm 0.014 \pm 0.021$	$0.705 \pm 0.011 \pm 0.019$	$0.611 \pm 0.015 \pm 0.022$
2.75–3.14	$0.789 \pm 0.013 \pm 0.024$	$0.671 \pm 0.010 \pm 0.020$	$0.620 \pm 0.015 \pm 0.026$

Table III. Values of R_{2h} obtained for each target and each $m_{\pi\pi}$ bin \pm the statistical uncertainty for each data point \pm the systematic uncertainty for each data point. These data correspond to those shown in Fig. 2(c)

$m_{\pi\pi}$ [GeV]	$R_{2h}(\text{C}, m_{\pi\pi})$	$R_{2h}(\text{Fe}, m_{\pi\pi})$	$R_{2h}(\text{Pb}, m_{\pi\pi})$
0.30–0.44	$1.021 \pm 0.057 \pm 0.035$	$0.914 \pm 0.041 \pm 0.031$	$0.836 \pm 0.066 \pm 0.030$
0.44–0.58	$0.962 \pm 0.030 \pm 0.046$	$0.896 \pm 0.023 \pm 0.043$	$0.874 \pm 0.037 \pm 0.042$
0.58–0.72	$0.920 \pm 0.019 \pm 0.023$	$0.813 \pm 0.015 \pm 0.021$	$0.798 \pm 0.023 \pm 0.020$
0.72–0.86	$0.878 \pm 0.013 \pm 0.023$	$0.782 \pm 0.010 \pm 0.020$	$0.782 \pm 0.016 \pm 0.020$
0.86–1.00	$0.831 \pm 0.014 \pm 0.023$	$0.721 \pm 0.011 \pm 0.020$	$0.670 \pm 0.016 \pm 0.018$
1.00–1.14	$0.769 \pm 0.015 \pm 0.021$	$0.685 \pm 0.012 \pm 0.019$	$0.604 \pm 0.017 \pm 0.017$
1.14–1.28	$0.834 \pm 0.018 \pm 0.026$	$0.725 \pm 0.015 \pm 0.023$	$0.647 \pm 0.021 \pm 0.020$
1.28–1.42	$0.913 \pm 0.028 \pm 0.035$	$0.782 \pm 0.023 \pm 0.030$	$0.734 \pm 0.033 \pm 0.028$
1.42–1.56	$0.952 \pm 0.049 \pm 0.046$	$0.913 \pm 0.043 \pm 0.044$	$0.716 \pm 0.054 \pm 0.041$
1.56–1.70	$1.410 \pm 0.116 \pm 0.095$	$1.173 \pm 0.089 \pm 0.079$	$1.092 \pm 0.124 \pm 0.094$